

A Model-independent Method to Determine H_0 Using Time-Delay Lensing, Quasars and Type Ia Supernovae

XIAOLEI LI,¹ RYAN E. KEELEY,² ARMAN SHAFIELOO,^{3,4} AND KAI LIAO⁵

¹*College of Physics, Hebei Normal University, Shijiazhuang 050024, People's Republic of China*

²*Department of Physics, University of California Merced, 5200 North Lake Road, Merced, CA 95343, USA*

³*Korea Astronomy and Space Science Institute, Daejeon 34055, Republic of Korea*

⁴*University of Science and Technology, Yuseong-gu 217 Gajeong-ro, Daejeon 34113, Republic of Korea*

⁵*School of Physics and Technology, Wuhan University, Wuhan 430072, People's Republic of China*

(Dated: January 8, 2024)

ABSTRACT

Absolute distances from strong lensing can anchor Type Ia Supernovae (SNe Ia) at cosmological distances giving a model-independent inference of the Hubble constant (H_0). Future observations could provide strong lensing time-delay distances with source redshifts up to $z \simeq 4$, which are much higher than the maximum redshift of SNe Ia observed so far. In order to make full use of time-delay distances measured at higher redshifts, we use quasars as a complementary cosmic probe to measure cosmological distances at redshifts beyond those of SNe Ia and provide a model-independent method to determine H_0 . In this work, we demonstrate a model-independent, joint constraint of SNe Ia, quasars, and time-delay distances from strong lensed quasars. We first generate mock data sets of SNe Ia, quasar, and time-delay distances based on a fiducial cosmological model. Then, we calibrate the quasar parameters model independently using Gaussian process (GP) regression with mock SNe Ia data. Finally, we determine the value of H_0 model-independently using GP regression from mock quasars and time-delay distances from strong lensing systems. As a comparison, we also show the H_0 results obtained from mock SNe Ia in combination with time-delay lensing systems whose redshifts overlap with SNe Ia. Our results show that quasars at higher redshifts show great potential to extend the redshift coverage of SNe Ia and thus enable the full use of strong lens time-delay distance measurements from ongoing cosmic surveys and improve the accuracy of the estimation of H_0 from 2.1% to 1.3% when the uncertainties of the time-delay distances are 5% of the distance values.

Keywords: Unified Astronomy Thesaurus concepts: Hubble constant (758); Observational cosmology (1146); Strong gravitational lensing (1643); Hubble diagram (759)

1. INTRODUCTION

The simplest flat Λ CDM model explains a large range of current observations including cosmic microwave background radiation (CMB), Big Bang nucleosynthesis and baryon acoustic oscillation (BAO) measurements (Schlegel et al. 2009; Ade et al. 2014, 2016; Aghanim et al. 2020; Alam et al. 2021). However, there are significant tensions between different data sets when Λ CDM is used to estimate some key cosmological parameters. One of the major issues is the discrepancy between the value of the Hubble constant measured by the multiple local-universe probes (Riess et al. 2018, 2019; Reid et al. 2019; Riess et al. 2022) and that inferred by early-universe probes under the assumption of Λ CDM cosmology (Aghanim et al. 2020). This tension has reached the 4σ to 6σ level (Di Valentino et al. 2021).

The tension either could be due to unknown systematic errors in the observations or could reveal new physics beyond Λ CDM. A model-independent method to determine H_0 from observations in the redshift gap between local-universe probes and early-universe probes is necessary to better assess the H_0 tension. Quasars are luminous persistent sources in the Universe which can be observed up to redshifts of $z \simeq 7.5$ (Mortlock et al. 2011). The magnifying effect of strong gravitational lensing can be used to observe quasars at even higher redshifts. With future surveys, the redshift of SNe Ia from Nancy Grace Roman Space Telescope (ROMAN) SN could reach $z \sim 2$ with larger uncertainties (Hounsell et al. 2023). On the other hand, future surveys will provide us with more strong lensing system measurements with higher redshift (Oguri & Marshall 2010). There-

fore, lensed quasars act as a potential cosmic probe at higher redshifts to shrink the redshift gap between the farthest observed SN Ia and CMB observations.

Recently, a feasible method to determine H_0 independent of the cosmological model that used strong lensed quasars and Type Ia supernovae (SNe Ia) with Gaussian Process (GP) regression has been presented in Liao et al. (2019, 2020). Strong gravitational lensing of a variable source measures the time-delay distance $D_{\Delta t}$ of the system and measuring the stellar velocity dispersion of the lens also yields a constraint on the angular diameter distance to the lens D_d . One can anchor SNe Ia with these absolute distances and obtain an excellent constraint on the shape of the distance-redshift relation (Collett et al. 2019). In Liao et al. (2019, 2020), the authors applied GP regression to SNe Ia data to get a model-independent relative distance-redshift relation and anchored the distance-redshift relation with $D_{\Delta t}$ and D_d from strong gravitational lensing to give the constraints on H_0 .

However, observations of strong lens systems summarized in Schmidt et al. (2023) show that the redshift of lensed quasars could reach as high as $z \simeq 3.8$, which is far beyond the highest redshift of observed SNe Ia so far. Therefore, looking for observations at higher redshifts is necessary to make full use of time-delay lensing systems. Recently Du et al. (2023) used gamma-ray burst (GRB) distances and H0LiCOW lenses with redshifts < 1.8 to infer H_0 .

Moreover, the linear relation between the log of the UV and X-ray luminosities allows quasars to be potentially used as standard candles at higher redshifts if well calibrated (Risaliti & Lusso 2015; Lusso & Risaliti 2017; Risaliti & Lusso 2019; Lusso et al. 2020; Khadka & Ratra 2021, 2020; Li et al. 2021). Thus, the combination of time-delay observations in strong lensed quasars and the linear relation between the log of the ultraviolet (UV) and X-ray luminosities of quasars can help us to determine H_0 model-independently.

In our work, we use GP regression to reconstruct the expansion history of the Universe model-independently. We first generate SNe Ia, quasar, and strong lens data set based on a fiducial cosmological model. Then, we calibrate the mock quasar data set by using GP regression to model-independently reconstruct the expansion history of the Universe from the mock SNe Ia data set following the previous work by (Li et al. 2021). Using the calibrated quasar data set, we further reconstruct the expansion history up to redshift of $z \simeq 7.5$ with GP. Then following Liao et al. (2019, 2020) we determine H_0 cosmological-model-independently using simu-

lated strong lensed quasars with source redshifts up to 4 and calibrated unlensed quasars.

This paper is organized as follows: in Section 2, we describe the data sets we used in detail. The quasar calibration with GP regression from the latest SNe Ia observations, as well as the determination of H_0 from strong lens systems and calibrated quasars are shown in Section 3. We discuss our conclusions in Section 4.

2. DATA

Since there is a lack of necessary time-delay measurements for strong lensing systems, we are going to simulate the time-delay measurements based on a fiducial cosmological model. Moreover, to make the results convective, we use simulated SNe Ia data as well as simulated quasar samples instead of the real data from observations.

In this section, we briefly describe the method of generating the mock data based on a fiducial cosmological model. Throughout our work, a flat- Λ CDM model with $\Omega_m = 0.3$ and $H_0 = 70 \text{ km s}^{-1} \text{ Mpc}^{-1}$ is used as the fiducial cosmological model. We should emphasize here that following our previous works, we could have selected any cosmological model (as the fiducial model) for our analysis since we are performing a model-independent analysis for reconstructing the expansion history. We have chosen the standard flat- Λ CDM model as our fiducial model since the focus of this paper is on the high precision determination of H_0 using high redshift quasars.

2.1. Type Ia Supernovae

SNe Ia, which helped discover cosmic acceleration, are powerful standard candles that enable precise measurements of the expansion of the Universe. A most recent Pantheon+ sample was reported in (Scolnic et al. 2022) which consists of 1701 light curves of 1550 distinct SNe Ia ranging in redshift from $z=0.001$ to 2.26. This larger SNe Ia sample is a significant increase compared to the original Pantheon sample, especially at lower redshifts.

In this work, we generate a mock SNe Ia data set based on the Pantheon+ sample assuming a fiducial cosmological model. First, we obtain the luminosity distances of SNe Ia with

$$D_L^{\text{fid}}(z) = \frac{c(1+z)}{H_0} \int_0^z \frac{dz}{\sqrt{\Omega_m(1+z)^3 + (1-\Omega_m)}} \quad (1)$$

and then the distance modulus can be calculated with

$$\mu^{\text{fid}} = 5 \log\left(\frac{D_L^{\text{fid}}}{1 \text{ Mpc}}\right) + 25. \quad (2)$$

The mock SNe Ia data, μ^{mock} , are then generated from μ^{fid} by adding noise as a random variable with a mean

of zero and a variance characterized by the Pantheon+ covariance matrix. We use this mock SNe Ia data set along with the mock quasar data set to simultaneously calibrate the mock quasar data set and reconstruct the Universe’s expansion history.

2.2. Quasar sample

Quasars act as standard candles based on the log-linear relation between the UVt and the X-ray luminosities $\log(L_X) = \gamma \log(L_{UV}) + \beta_1$. This allows quasars to work as cosmic probes at higher redshifts to shrink the redshift gap between SNe Ia and the CMB if well calibrated since they can be observed up to the redshifts of $z \simeq 7.5$. So far, the largest quasar sample with both X-ray and UV observations consists of $\sim 12,000$ objects. However, after applying several filtering steps to reduced the systematic effects, 2421 quasars with spectroscopic redshifts and X-ray observations from either Chandra or XMM–Newton in the redshift range of $0.009 < z < 7.54$ were left in the final cleaned sample (Lusso et al. 2020).

In this work, we generate a mock quasar data set based on the quasar catalog described above assuming a fiducial cosmological model. First, we take the values of $\log(F_{UV})^{\text{fid}}$ from the actual measurements. Then, we calculate $\log(F_X)^{\text{fid}}$ using

$$\log(F_X)^{\text{fid}} = \gamma \log(F_{UV})^{\text{fid}} + (2\gamma - 2)\log(D_L^{\text{fid}}) + \beta_2 \quad (3)$$

where $\beta_2 = \gamma \log(4\pi) - \log(4\pi) + \beta_1$, F_{UV} and F_X are the fluxes measured at fixed rest-frame wavelengths, and D_L^{fid} is the luminosity distance relation of the fiducial cosmology. γ and β_2 are quasar parameters that need to be calibrated. These calibration parameters are degenerate with the cosmological parameters, or model-independent distances we want to fit or reconstruct. Since β_2 is degenerate with H_0 , quasars can only measure relative distances, just like SNe Ia. Thus, we absorb H_0 into the parameter $\beta = \beta_2 - (2\gamma - 2)\log(H_0)$. This is to absorb multiple degenerate parameters which characterize the relative anchoring between the data and the expansion history into one parameter. Here, we use fiducial values for $\gamma = 0.6430$ and $\beta = 7.88$, which are the best-fit values from Li et al. (2021). The final sample of fluxes ($\log(F_{UV})^{\text{mock}}$, $\log(F_X)^{\text{mock}}$) are calculated from the fiducial values ($\log(F_{UV})^{\text{fid}}$, $\log(F_X)^{\text{fid}}$) by adding Gaussian random noise with a standard deviation ($\sigma_{\log(F_{UV})}$, $\sigma_{\log(F_X)}$) from the actual data set.

2.3. Strong lens time-delay distance data

A typical strongly lensed system, as used for time-delay cosmography, consists of a source quasar at cosmological distances, which is lensed by a foreground elliptical galaxy, and forms multiple images of the quasar

and the arcs of the host galaxy. With years of observations of the light curves, one can measure the time delay between any two images, which, following the Fermat principle, arises from the different geometries and Shapiro time delays along the multiple paths. The time delay thus depends on both the geometry of the Universe and the gravitational field of the lens galaxy. The time delays Δt can be used to measure a time-delay distance $D_{\Delta t}$ following

$$\Delta t = D_{\Delta t} \Delta\phi(\xi_{\text{lens}}) \quad (4)$$

where $\Delta\phi$ is the Fermat potential difference between the two images which is a function of lens mass profile parameters ξ_{lens} , determined by high-resolution imaging of the host arcs. $D_{\Delta t}$ is the time-delay distance

$$D_{\Delta t} = (1 + z_d) \frac{D_d D_s}{D_{ds}} \quad (5)$$

which is a combination of three angular diameter distances D_d , D_s , and D_{ds} where the subscripts d and s denotes the deflector (lens) and the source, respectively. Time-delay distance measurements can be used as a one-rung distance ladder and are independent of the Cepheid distance ladder and early Universe physics. The angular diameter distance to the deflector lens itself, D_d , can be obtained independently of the time-delay distance of the strong lens system. These D_d measurements provide additional constraints on the expansion history beyond the $D_{\Delta t}$ measurements.

With the increasing number of the wide-field imaging surveys, e.g., Vera C. Rubin Observatory’s Legacy Survey of Space and Time (LSST), Euclid, and ROMAN, the number of the known strong lens systems is growing rapidly (Spergel et al. 2015; Akeson et al. 2019; Oguri & Marshall 2010; Collett 2015). New images of billions of galaxies are expected to be observed, of which $\sim 100,000$ are strong lens systems (Collett 2015).

In this work, we simulate angular diameter distances and time-delay distances for each strong lens system following the method described below:

1. In the fiducial cosmological model, the angular diameter distance can be calculated via

$$D_A^{\text{fid}}(z) = D_L^{\text{fid}} / (1 + z)^2 \quad (6)$$

with the redshift to the deflector z_d and the redshift to the source z_s , we can calculate D_d and D_s , respectively. Random noise following a normal distribution is added to the angular diameter distance. We analyze two cases, one where the noise being added is at the level of 5% and another at the level of 10%. The value depends on specific

systems, observational conditions, algorithm and most importantly systematical errors. We adopted 5% for the best case and 10% for the worse case.

In a spatially flat universe, the distance between the lens and the source (D_{ds}) is calculated via

$$D_{\text{ds}} = D_s - \frac{1 + z_d}{1 + z_s} D_d. \quad (7)$$

2. Then, the time-delay distance can be obtained with Equation (5).
3. We consider two cases, where the uncertainties on the simulated distances (both D_d and $D_{\Delta t}$) are taken to be 5% and 10%.

In this work, we use nine mock strongly lensed quasars based on those in Ertl et al. (2023) which is a subset of 30 quadruply imaged quasars in Schmidt et al. (2023). The sample will probably be analyzed by the TDCOSMO team in the next stage (Treu et al. 2022). The redshifts of strong lens systems are summarized in Table 1 which is part of Table A.3 from Ertl et al. (2023). These systems have higher source redshifts than H0LiCOW and might be well analyzed by the TDCOSMO team in the near future. The boldface shows the lensing systems whose redshifts in the redshift range of SNe Ia ($z < 2.261$). As can be seen from Table 1, only three strong lens systems are left in the redshift coverage of SNe Ia.

Following the simulation method described above, we obtain the simulated angular diameter distance to the lens and the time-delay distance, which are shown in the last two columns of Table 1. Throughout our work, we consider 5% and 10% of distance values as uncertainties for the mock time-delay distance $D_{\Delta t}$ and angular diameter distance to the deflector D_d .

We show the redshift distribution for the data set used in our analysis in Figure 1.

3. METHODS AND RESULTS

3.1. Quasar calibration

In this subsection, we briefly describe the method we used to simultaneously calibrate the quasar sample and reconstruct the expansion history using the SNe Ia data set and GP regression.

In order to calibrate the quasar parameters in a model-independent way, we use cosmological distances from another cosmic probe – SNe Ia. Since the absolute brightness of SNe Ia is degenerate with H_0 , only the dimensionless, unanchored luminosity distances ($D_L H_0$) can be constrained. We rewrite Eq. (3) as

$$\log(F_X) = \gamma \log(F_{\text{UV}}) + (2\gamma - 2) \log(D_L H_0) + \beta \quad (8)$$

Table 1. The deflector and source redshifts and the simulated angular diameter distance and time-delay distance for our strong lens systems. We denote lensing systems whose redshifts are overlap with the redshifts of SNe Ia ($z < 2.261$) in boldface.

System	z_d	z_s	D_d	$D_{\Delta t}$
DES J0029-3814	0.863	2.821	1523.3	6315.0
DES J0214-2105	0.22	3.229	801.4	988.6
DES J0420-4037	0.358	2.4	1030.8	1907.7
PS J0659+1629	0.766	3.083	1420.3	4976.3
2M1134-2103	0.5	2.77	1273.9	2732.5
J1537-3010	0.592	1.721	1326.7	4199.4
PS J1606-2333	0.5	1.69	1234.7	3562.1
PS J1721+8842	0.184	2.37	628.9	838.8
DES J2100-4452	0.203	0.92	780.0	935.5

where $\beta = \beta_2 - (2\gamma - 2) \log(H_0)$. $D_L H_0$ is reconstructed from the mock SNe Ia data set using GP regression. GP regression works by generating a random set of cosmological functions whose statics are characterized by a covariance function. We follow some previous works and use a squared-exponential kernel for the covariance function (Rasmussen & Williams 2006; Holsclaw et al. 2010a,b; Holsclaw et al. 2011; Shafieloo et al. 2012; Shafieloo et al. 2013; Joudaki et al. 2018; Hwang et al. 2023)

$$\langle \varphi(s_i) \varphi(s_j) \rangle = \sigma_f^2 \exp\left(-\frac{|s_i - s_j|^2}{2\ell^2}\right) \quad (9)$$

where $s_i = \ln(1 + z_i) / \ln(1 + z_{\text{max}})$ and $z_{\text{max}} = 2.261$ is the maximum redshift of the SNe Ia sample. σ_f and ℓ are two hyperparameters that are marginalized over. φ is just a random function drawn from the distribution defined by the covariance function of Equation (9) and we take this function as $\varphi(z) = \ln(H^{\text{mf}}(z)/H(z))$, i.e. the logarithm of the ratio between the reconstructed expansion history, $H(z)$, and a mean function, $H^{\text{mf}}(z)$, which we choose to be the best-fit Λ CDM model from the Pantheon+ data set. The mean function plays an important role in GP regression and the final reconstruction results are not quite independent of the mean function, however, it has a modest effect on the final reconstruction results because the values of hyperparameters help to trace the deviations from the mean function (Shafieloo et al. 2012; Shafieloo et al. 2013; Aghamousa et al. 2017). Moreover, the true model should be very close to the flat Λ CDM model so it is reasonable to choose the best-fit flat Λ CDM model from Pantheon+ as a mean function. This choice allows us to perform a test of whether the data need some additional flexibility to fit the data beyond the Λ CDM model (Keeley et al. 2021).

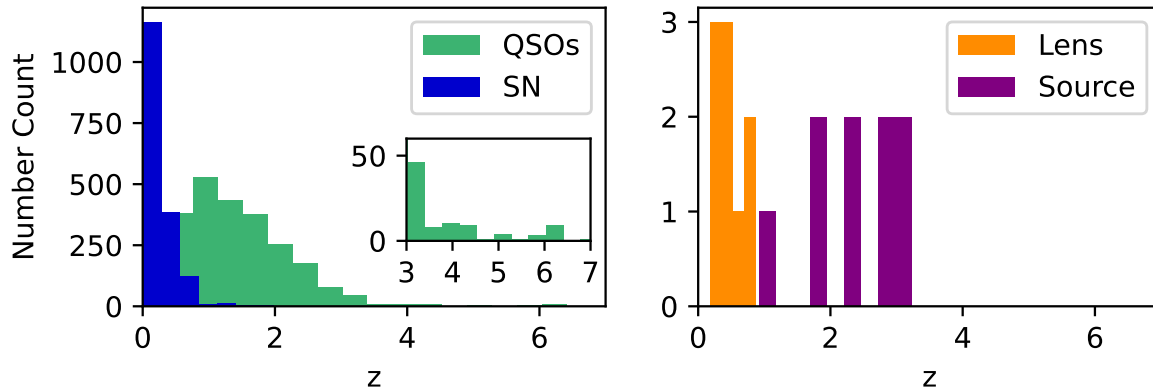


Figure 1. The left plot shows the redshift distribution of the Quasar sample from Lusso et al. (2020) and SNe Ia from Pantheon+ sample (Scolnic et al. 2022) while the right plot shows the redshift distribution of the sources and deflector for the strong lens time-delay data set from Ertl et al. (2023). The redshift distribution of quasars at higher redshift are also displayed in the inner plot to make it more clear.

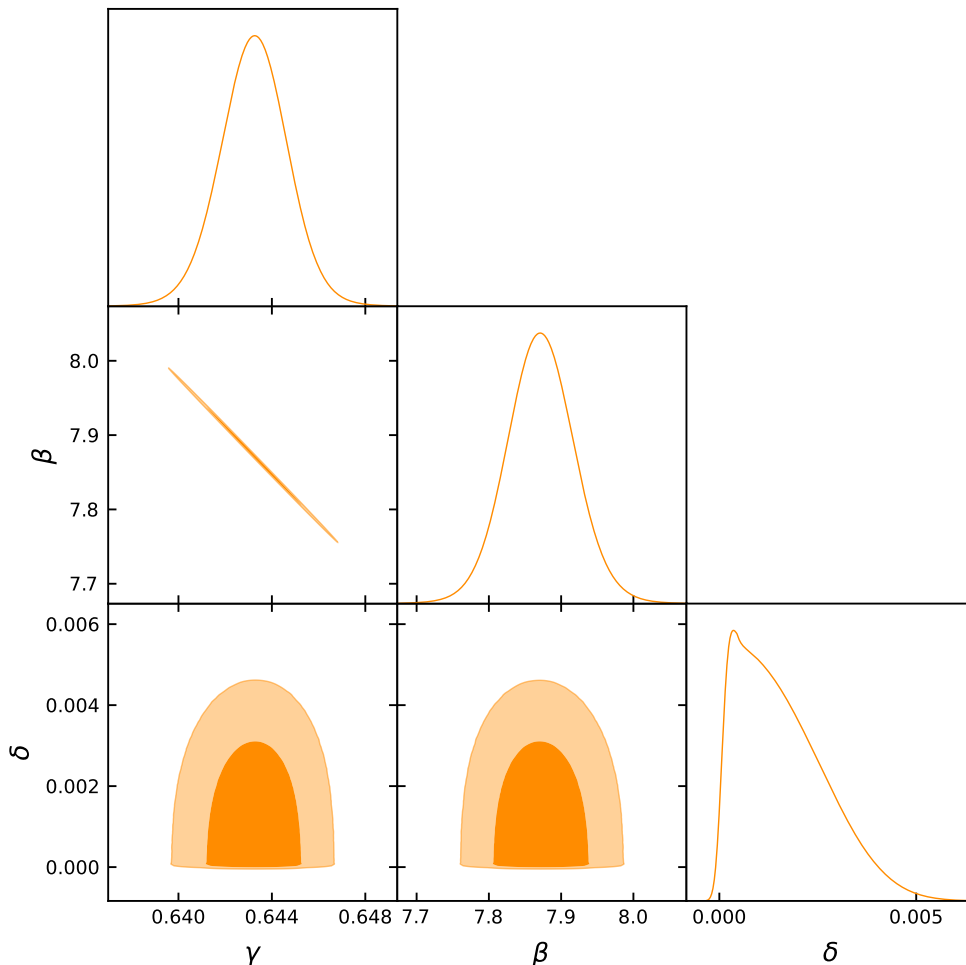


Figure 2. Model-independent calibration results for the quasar parameters, where γ is the slope of the log-linear relation between the UV and X-ray luminosity of quasars and β relates to the intercept of the relation. While δ is the intrinsic scatter of quasars. GP reconstructions of $D_L H_0$ based on the mock SNe Ia data. The contours represent the 1σ and 2σ uncertainties for γ , β , and δ .

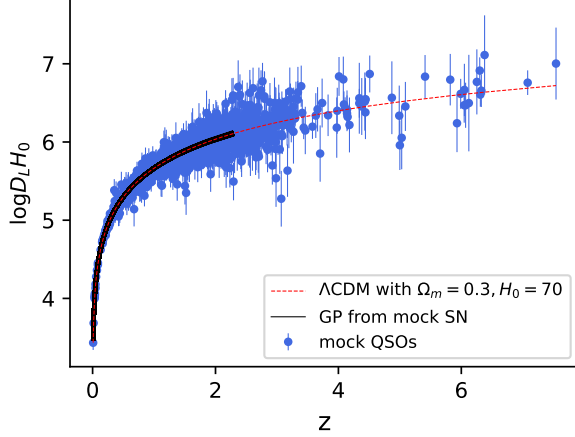


Figure 3. $\log(D_L H_0)$ -redshift relation for the mock quasars. The errorbars of $\log(D_L H_0)$ are obtained through error propagation and the black solid lines show $\log(D_L H_0)$ obtained from mock SNe Ia data and the dashed red line denotes flat Λ CDM model with $H_0 = 70 \text{ km s}^{-1} \text{ Mpc}^{-1}$ and $\Omega_m = 0.3$ as comparison.

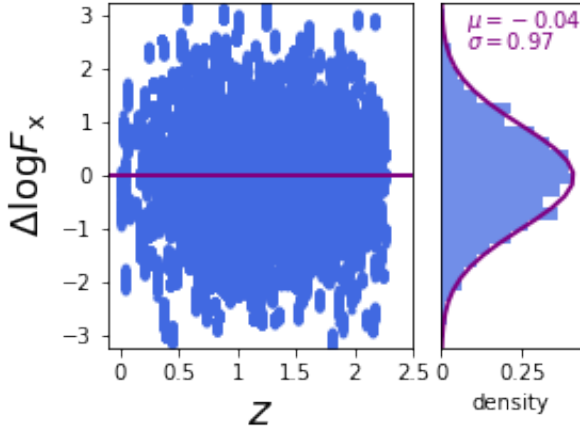


Figure 4. Residuals of the mock $\log(F_X)$ values with respect to the predicted $\log(F_X)$ values derived from the GP reconstructions of the mock SNe Ia compilation, normalized to the calibrated errors (observational and intrinsic). The right plot shows the histogram for $\Delta \log(F_X)$ and the purple line shows the best Gaussian fit with $\mu = -0.04$ and $\sigma = 0.97$.

For the details of the reconstruction with GP, we refer the readers to (Rasmussen & Williams 2006; Holsclaw et al. 2010a,b; Holsclaw et al. 2011; Shafieloo et al. 2012; Shafieloo et al. 2013; Aghamousa et al. 2017; Keeley et al. 2021; Li et al. 2021; Hwang et al. 2023).

With the measurements of F_{UV} from the quasar sample and $D_L H_0$ from SNe Ia, we obtain $\log(F_X)^{\text{SN}}$ following Equation (8). This allows us to compare the quasar

data set and the SNe Ia data set with

$$\ln \mathcal{L} = -\frac{1}{2} \sum_i \left[\frac{\left(\log(F_X(\gamma, \beta))_i^{\text{SN}} - \log(F_X)_i^{\text{QSO}} \right)^2}{s_i^2} + \ln(s_i^2) \right] \quad (10)$$

where $s_i^2 = \sigma_{\log(F_X)}^2 + \gamma^2 \sigma_{\log(F_{UV})}^2 + \delta^2$. The intrinsic dispersion δ of the $L_X - L_{UV}$ relation models various unknown physical properties that scatter the observed $\log(L_X)$ - $\log(L_{UV})$ trend by more than the measurement uncertainty (Risaliti & Lusso 2019; Lusso et al. 2020).

We then calculate the posterior distribution of the quasar parameters: the slope γ , the intercept β and the intrinsic dispersion parameter δ . We should note that the Hubble constant H_0 is absorbed into the parameter β . This is to absorb multiple degenerate parameters that characterize the relative anchoring between the data and the expansion history into one parameter. Based on the method described above, we use a Python package named *emcee* (Foreman-Mackey et al. 2013) to do the Markov Chain Monte Carlo analysis and flat priors are used for each parameter.

With the calibration method described above, we obtained the best fit of quasar parameters, $\gamma = 0.643 \pm 0.002$, $\beta = 7.872 \pm 0.047$ and $\delta = 0.0016_{-0.0015}^{+0.0006}$ and the contours are shown in Figure 2.

To make sure that our calibrated results give reasonable information about cosmology, we calculate $\log(D_L H_0)$ versus z relation from the quasar fluxes with the calibrated quasar parameters through

$$\log(D_L H_0) = \frac{\log(F_X) - \gamma \log(F_{UV}) - \beta}{(2\gamma - 2)}. \quad (11)$$

The results are shown in Figure 3. The blue points represent the unanchored distances from the calibrated quasar sample, which we use to anchor time-delay distances of strong lensing in later work. In Figure 3 we also show the $\log(D_L H_0)$ obtained from the posterior of SNe Ia calculated with GP.

Moreover, we check the consistency between the calibrated quasar sample and the unanchored luminosity distance from SNe Ia by estimating the normalized residual of $\log(F_X)^{\text{SN}}$ which is calculated via

$$\Delta \log(F_X) = \frac{\log(F_X)^{\text{SN}} - \log(F_X)^{\text{QSO}}}{\sqrt{\sigma_{\log(F_X)}^2 + \gamma^2 \sigma_{\log(F_{UV})}^2 + \delta^2}}. \quad (12)$$

where $\log(F_X)^{\text{SN}}$ is obtained with Equation (8) and $\log(F_X)^{\text{QSO}}$ is the quasar measurements. The results for the residual are shown in Figure 4. From Figure 4

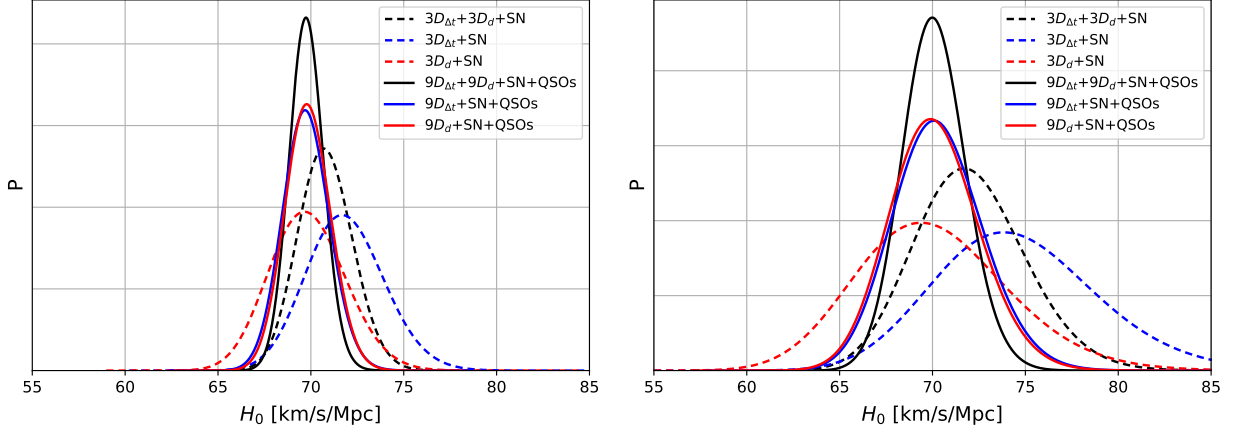


Figure 5. The posterior on H_0 obtained with simulated time-delay lensing distance ($D_{\Delta t}$) as well as lensing distance (D_d). The left plot denotes the results with 5% uncertainties of the simulated distance values and the right plot denotes the results with 10% uncertainties when doing simulation.

we can see that the distribution of the normalized residual is a Gaussian distribution, which indicates that the $\log(F_X)$ data from quasar measurements is consistent with that derived from SNe Ia using calibrated quasar parameters.

Finding internal consistency between the calibrated quasar and SNe Ia data sets would show that quasars can be used as standard candles at higher redshift and are therefore powerful probes of cosmology. We also need to emphasize here that there are deviations from the standard Λ CDM model for quasars at higher redshift as standard candles. It is not clear so far that whether the deviations are due to new physics beyond the Λ CDM model or the evolution of calibration parametrizations. Hopefully, future surveys will provide us more copious and precise data for quasars which could help us solve this puzzle.

3.2. H_0 determination

In order to determine H_0 with our technique, we have to take the unanchored reconstructions of the expansion history from SNe Ia and quasars, which only measure relative distances, and anchor them with the strong lens data set, which does measure absolute distances. We first generate 1000 posterior samples of the H_0 -independent quantity $D_L H_0$ from quasars with GP regression mentioned above and convert these unanchored luminosity distances to unanchored angular diameter distances $D^A H_0$. Then we evaluate the values of each of the 1000 $D^A H_0$ curves at the lens and the source redshifts of the simulated strong lens systems to calculate 1000 values of $H_0 D_{\Delta t}$ using

$$H_0 D_{\Delta t} = (1 + z_d) \frac{(H_0 D_d)(H_0 D_s)}{(H_0 D_{ds})} \quad (13)$$

where $D_{\Delta t}$ is the time-delay distance. Comparing 1000 $H_0 D_{\Delta t}$ and $H_0 D_d$ curves with simulated $D_{\Delta t}$ and D_d at the lens and source redshifts of the lensing systems, we calculate the likelihood with

$$(\ln \mathcal{L})_{D_{\Delta t}} = -\frac{1}{2} \sum \frac{\frac{H_0 D_{\Delta t}}{H_0}(H_0; z_d, z_s) - D_{\Delta t}^{\text{sim}}(z_d, z_s)}{\sigma_{D_{\Delta t}}(z_d, z_s)} \quad (14)$$

and

$$(\ln \mathcal{L})_{D_d} = -\frac{1}{2} \sum \frac{\frac{H_0 D_d}{H_0}(H_0; z_d) - D_d^{\text{sim}}(z_d)}{\sigma_{D_d}(z_d)} \quad (15)$$

In the end, we marginalize over the realizations to form the posterior distribution of H_0 .

The posterior on H_0 in a flat Λ CDM model obtained with nine simulated strong lens systems in combination with quasars and SNe Ia are shown in solid lines in Figure 5. The left plot shows the H_0 estimation results taking 5% of the distance values as uncertainties while the right plot shows the H_0 estimation results taking 10% of the distance values as uncertainties. In Table 2 we summarize the numerical results. First, we consider the combination of $D_{\Delta t}$ and D_d from the nine simulated lensing systems. The method described above yields $H_0 = 69.8 \pm 0.9 \text{ km s}^{-1} \text{ Mpc}^{-1}$ when taking 5% of the distance values as uncertainties and $H_0 = 70.1 \pm 1.7 \text{ km s}^{-1} \text{ Mpc}^{-1}$ when taking 10% of the distance values as uncertainties. In addition, we give the results from D_d and $D_{\Delta t}$ separately to quantify the contribution of D_d in Figure 5. The constraints when the angular diameter distances to the lens deflector (D_d) are considered separately from the time-delay distances ($D_{\Delta t}$) are largely equivalent. We can also see from Figure 5 that the constraining power of the combination of D_d and $D_{\Delta t}$ will improve a lot compared to the results from D_d and $D_{\Delta t}$ separately.

Table 2. The best-fit values for H_0 and the corresponding 1σ uncertainties as well as the precision of the estimation when the precision of the measurement of the distances in the strong lens data set is 5% and 10%. For comparison, we include the case where we are limited to using the strong lens systems with source redshifts within the SNe Ia redshift range.

data	5% Uncertainties		10% Uncertainties	
	Best-fit Values	Precision	Best-fit Values	Precision
$9D_d + 9D_{\Delta t} + \text{SN} + \text{QSO}$	69.8 ± 0.9	1.3%	70.1 ± 1.7	2.4%
$3D_d + 3D_{\Delta t} + \text{SN}$	70.8 ± 1.5	2.1%	$72.0^{+2.7}_{-3.2}$	4.1%
$9D_{\Delta t} + \text{SN} + \text{QSO}$	69.7 ± 1.3	1.8%	$70.3^{+2.2}_{-2.6}$	3.4%
$3D_{\Delta t} + \text{SN}$	$71.9^{+2.0}_{-2.2}$	3.0%	$74.6^{+3.8}_{-4.8}$	5.8%
$9D_d + \text{SN} + \text{QSO}$	69.8 ± 1.2	1.7%	$70.1^{+2.2}_{-2.5}$	3.4%
$3D_d + \text{SN}$	$69.8^{+1.9}_{-2.1}$	3.0%	$70.1^{+3.6}_{-4.5}$	5.8%

As a comparison, we also use SNe Ia as standard candles following the same H_0 determination method described above to determine H_0 model-independently. However, only three strong lens systems are left in the redshift range of SNe Ia. The constraints are shown in dashed lines in Figure 5 and the best-fit values together with the 1σ uncertainties are summarized in Table 2. We obtain $H_0 = 70.8 \pm 1.5 \text{ km s}^{-1} \text{ Mpc}^{-1}$ taking 5% of the distance values as uncertainties and $H_0 = 72.0^{+2.7}_{-3.2} \text{ km s}^{-1} \text{ Mpc}^{-1}$ taking 10% of the distance values as uncertainties with three time-delay lensing systems in combination with SNe Ia. We see that by using quasars and not just SNe Ia as standard candles, more time-delay lensing systems can be included because quasars are measured out to higher redshift, thus yielding a tighter constraint on H_0 . The precision of estimating H_0 can be improved from 2.1% to 1.3% with adding quasars as standard candles when the uncertainties of the time-delay distances are 5%.

4. CONCLUSION AND DISCUSSIONS

In this work, we develop a model-independent method to measure the Hubble constant with time-delay distances from strong lens systems combined with quasar and SNe Ia standard candles.

We first generate mock data sets of SNe Ia, quasars, and strong lenses based on a fiducial cosmological model. Then we apply our GP regression technique on the mock SNe Ia and quasar data sets to simultaneously calibrate the mock quasar data set and reconstruct the Universe’s expansion history. This reconstruction extends out to a redshift of 7.5, further than any other reconstruction to date. We also demonstrate how to test the reliability of our calibrated results, namely by calculating the normalized residuals of the $\log F_X$ with respect to the mock SNe Ia data set. If the normalized residuals follow a Gaussian distribution, then the calibration results are reliable.

Since both the quasar and SNe Ia data sets are unanchored, we then anchor the reconstruction of expansion

history from those data sets with the time-delay distances from the mock strong lens data set. Previous model-independent reconstructions of the expansion history have only used SNe Ia. Since SNe Ia only extend to a redshift of 2.26, the model-independent reconstructions can only use the three strong lens systems with source redshifts less than 2.26. Using quasar as standard candles extends the redshift coverage over our model-independent reconstruction, and thus we can use nine strong lens systems in our analysis. This yields a 1.3% precision on H_0 in an optimistic case (5% precision for strong lens distances) for a future strong lens data set and 2.4% precision in a less optimistic case (10% precision).

Fortunately, we will obtain more well-measured time-delay strong lens systems with the onset of cosmic surveys such as Roman, LSST, and Euclid. In addition to lensed quasars, strongly lensed transients, such as SN, are coming soon (Liao et al. 2022). With future time-delay distance measurements together with a larger and more precise quasar data set, one can obtain H_0 more precisely with the method described in this work and understand the H_0 tension better.

ACKNOWLEDGEMENTS

KL was supported by National Natural Science Foundation of China (NSFC) No. 12222302, 11973034 and y Funds for the Central Universities (Wuhan University 1302/600460081). X.Li was supported by NSFC No. 12003006, Hebei NSF No. A2020205002 and the fund of Hebei Normal University No. L2020B02. A.S. would like to acknowledge the support by National Research Foundation of Korea NRF2021M3F7A1082053, and the support of the Korea Institute for Advanced Study (KIAS) grant funded by the government of Korea. This work benefits from the high performance computing clusters at College of Physics, Hebei Normal University.

REFERENCES

- Ade, P. A. R., et al. 2014, *Astron. Astrophys.*, 571, A16, doi: [10.1051/0004-6361/201321591](https://doi.org/10.1051/0004-6361/201321591)
- . 2016, *Astron. Astrophys.*, 594, A13, doi: [10.1051/0004-6361/201525830](https://doi.org/10.1051/0004-6361/201525830)
- Aghamousa, A., Hamann, J., & Shafieloo, A. 2017, *JCAP*, 2017, 031, doi: [10.1088/1475-7516/2017/09/031](https://doi.org/10.1088/1475-7516/2017/09/031)
- Aghanim, N., et al. 2020, *Astron. Astrophys.*, 641, A6, doi: [10.1051/0004-6361/201833910](https://doi.org/10.1051/0004-6361/201833910)
- Akeson, R., Armus, L., Bachelet, E., et al. 2019, arXiv e-prints, arXiv:1902.05569, doi: [10.48550/arXiv.1902.05569](https://doi.org/10.48550/arXiv.1902.05569)
- Alam, S., de Mattia, A., Tamone, A., et al. 2021, *MNRAS*, 504, 4667, doi: [10.1093/mnras/stab1150](https://doi.org/10.1093/mnras/stab1150)
- Collett, T., Montanari, F., & Räsänen, S. 2019, *PhRvL*, 123, 231101, doi: [10.1103/PhysRevLett.123.231101](https://doi.org/10.1103/PhysRevLett.123.231101)
- Collett, T. E. 2015, *ApJ*, 811, 20, doi: [10.1088/0004-637X/811/1/20](https://doi.org/10.1088/0004-637X/811/1/20)
- Collett, T. E. 2015, *Astrophys. J.*, 811, 20, doi: [10.1088/0004-637X/811/1/20](https://doi.org/10.1088/0004-637X/811/1/20)
- Di Valentino, E., Mena, O., Pan, S., et al. 2021, *Class. Quant. Grav.*, 38, 153001, doi: [10.1088/1361-6382/ac086d](https://doi.org/10.1088/1361-6382/ac086d)
- Du, S.-S., Wei, J.-J., You, Z.-Q., et al. 2023, *Mon. Not. Roy. Astron. Soc.*, 521, 4963, doi: [10.1093/mnras/stad696](https://doi.org/10.1093/mnras/stad696)
- Ertl, S., Schuldt, S., Suyu, S. H., et al. 2023, *Astron. Astrophys.*, 672, A2, doi: [10.1051/0004-6361/202244909](https://doi.org/10.1051/0004-6361/202244909)
- Foreman-Mackey, D., Hogg, D. W., Lang, D., & Goodman, J. 2013, *Publications of the Astronomical Society of the Pacific*, 125, 306
- Holsclaw, T., Alam, U., Sanso, B., et al. 2010a, *Phys. Rev. D*, 82, 103502, doi: [10.1103/PhysRevD.82.103502](https://doi.org/10.1103/PhysRevD.82.103502)
- . 2010b, *Phys. Rev. Lett.*, 105, 241302, doi: [10.1103/PhysRevLett.105.241302](https://doi.org/10.1103/PhysRevLett.105.241302)
- Holsclaw, T., Alam, U., Sansó, B., et al. 2011, *PhRvD*, 84, 083501, doi: [10.1103/PhysRevD.84.083501](https://doi.org/10.1103/PhysRevD.84.083501)
- Hounsell, R., Scolnic, D., Brout, D., et al. 2023. <https://arxiv.org/abs/2307.02670>
- Hwang, S.-g., L’Huillier, B., Keeley, R. E., Jee, M. J., & Shafieloo, A. 2023, *JCAP*, 2023, 014, doi: [10.1088/1475-7516/2023/02/014](https://doi.org/10.1088/1475-7516/2023/02/014)
- Joudaki, S., Kaplinghat, M., Keeley, R., & Kirkby, D. 2018, *PhRvD*, 97, 123501, doi: [10.1103/PhysRevD.97.123501](https://doi.org/10.1103/PhysRevD.97.123501)
- Keeley, R. E., Shafieloo, A., Zhao, G.-B., Vazquez, J. A., & Koo, H. 2021, *Astron. J.*, 161, 151, doi: [10.3847/1538-3881/abdd2a](https://doi.org/10.3847/1538-3881/abdd2a)
- Khadka, N., & Ratra, B. 2020, *Mon. Not. Roy. Astron. Soc.*, 497, 263, doi: [10.1093/mnras/staa1855](https://doi.org/10.1093/mnras/staa1855)
- . 2021, *Mon. Not. Roy. Astron. Soc.*, 502, 6140, doi: [10.1093/mnras/stab486](https://doi.org/10.1093/mnras/stab486)
- Li, X., Keeley, R. E., Shafieloo, A., et al. 2021, *Mon. Not. Roy. Astron. Soc.*, 507, 919, doi: [10.1093/mnras/stab2154](https://doi.org/10.1093/mnras/stab2154)
- Liao, K., Biesiada, M., & Zhu, Z.-H. 2022, *Chinese Physics Letters*, 39, 119801, doi: [10.1088/0256-307X/39/11/119801](https://doi.org/10.1088/0256-307X/39/11/119801)
- Liao, K., Shafieloo, A., Keeley, R. E., & Linder, E. V. 2019, *Astrophys. J. Lett.*, 886, L23, doi: [10.3847/2041-8213/ab5308](https://doi.org/10.3847/2041-8213/ab5308)
- . 2020, *Astrophys. J. Lett.*, 895, L29, doi: [10.3847/2041-8213/ab8dbb](https://doi.org/10.3847/2041-8213/ab8dbb)
- Lusso, E., & Risaliti, G. 2017, *Astron. Astrophys.*, 602, A79, doi: [10.1051/0004-6361/201630079](https://doi.org/10.1051/0004-6361/201630079)
- Lusso, E., et al. 2020, *Astron. Astrophys.*, 642, A150, doi: [10.1051/0004-6361/202038899](https://doi.org/10.1051/0004-6361/202038899)
- Mortlock, D. J., Warren, S. J., Venemans, B. P., et al. 2011, *Nature*, 474, 616, doi: [10.1038/nature10159](https://doi.org/10.1038/nature10159)
- Oguri, M., & Marshall, P. J. 2010, *MNRAS*, 405, 2579, doi: [10.1111/j.1365-2966.2010.16639.x](https://doi.org/10.1111/j.1365-2966.2010.16639.x)
- Rasmussen, C. E., & Williams, C. K. I. 2006, *The MIT Press*
- Reid, M. J., Pesce, D. W., & Riess, A. G. 2019, *The Astrophysical Journal Letters*, 886, L27, doi: [10.3847/2041-8213/ab552d](https://doi.org/10.3847/2041-8213/ab552d)
- Riess, A. G., Casertano, S., Yuan, W., Macri, L. M., & Scolnic, D. 2019, *The Astrophysical Journal*, 876, 85, doi: [10.3847/1538-4357/ab1422](https://doi.org/10.3847/1538-4357/ab1422)
- Riess, A. G., Casertano, S., Yuan, W., et al. 2018, *The Astrophysical Journal*, 855, 136, doi: [10.3847/1538-4357/aaadb7](https://doi.org/10.3847/1538-4357/aaadb7)
- Riess, A. G., et al. 2022, *Astrophys. J. Lett.*, 934, L7, doi: [10.3847/2041-8213/ac5c5b](https://doi.org/10.3847/2041-8213/ac5c5b)
- Risaliti, G., & Lusso, E. 2015, *Astrophys. J.*, 815, 33, doi: [10.1088/0004-637X/815/1/33](https://doi.org/10.1088/0004-637X/815/1/33)
- . 2019, *Nature Astron.*, 3, 272, doi: [10.1038/s41550-018-0657-z](https://doi.org/10.1038/s41550-018-0657-z)
- Schlegel, D., White, M., & Eisenstein, D. 2009, in *astro2010: The Astronomy and Astrophysics Decadal Survey*, Vol. 2010, 314. <https://arxiv.org/abs/0902.4680>
- Schmidt, T., et al. 2023, *Mon. Not. Roy. Astron. Soc.*, 518, 1260, doi: [10.1093/mnras/stac2235](https://doi.org/10.1093/mnras/stac2235)
- Scolnic, D., et al. 2022, *Astrophys. J.*, 938, 113, doi: [10.3847/1538-4357/ac8b7a](https://doi.org/10.3847/1538-4357/ac8b7a)
- Shafieloo, A., Kim, A. G., & Linder, E. V. 2012, *Physical Review D*, 85, 123530
- Shafieloo, A., Kim, A. G., & Linder, E. V. 2013, *PhRvD*, 87, 023520, doi: [10.1103/PhysRevD.87.023520](https://doi.org/10.1103/PhysRevD.87.023520)
- Spergel, D., Gehrels, N., Baltay, C., et al. 2015, arXiv e-prints, arXiv:1503.03757, doi: [10.48550/arXiv.1503.03757](https://doi.org/10.48550/arXiv.1503.03757)

Treu, T., Suyu, S. H., & Marshall, P. J. 2022, *Astron. Astrophys. Rev.*, 30, 8, doi: [10.1007/s00159-022-00145-y](https://doi.org/10.1007/s00159-022-00145-y)